

# Application of Single-cell Deep Learning in Elucidating the Mapping Relationship Between Visceral and Body Surface Inflammatory Patterns

**Authors:** Haixiang Huang<sup>1\*</sup>, Bingbing Shen<sup>1</sup>, Zhenwei Zhang<sup>1</sup>, Jianming Yue<sup>1</sup>, Lu Mei<sup>1</sup>, Qiusheng Chen<sup>1†</sup>

**Affiliations:**

<sup>1</sup>College of Veterinary Medicine, Nanjing Agricultural University, Nanjing, Jiangsu Province 210095, China

†Corresponding author. Email: chenqsh305@njau.edu.cn

**Abstract**

As a system of integrated homeostasis, life is susceptible to disruptions by visceral inflammation, which can disturb internal environment equilibrium. The role of body-spread subcutaneous fascia (scFascia) in this process is poorly understood. In the rat model of Salmonella-induced dysentery, scRNA-seq of scFascia and deep-learning analysis revealed Warburg-like metabolic reprogramming in macrophages (MPs) with reduced citrate cycle activity. Cd34+/Pdgfra+ telocytes (CPTCs) regulated MPs differentiation and proliferation via Wnt/Fgf signal, suggesting a pathological crosstalk pattern in the scFascia, herein termed the fascia-visceral inflammatory crosstalk pattern (FVICP). PySCENIC analysis indicated increased activity transcription factors Fosl1, Nfkb2, and Atf4, modulated by CPTCs signaling to MPs, downregulating aerobic respiration and upregulating cell cycle, DNA replication, and transcription. This study highlights scFascia's role in immunomodulation and metabolic reprogramming during visceral inflammation, underscoring its function in systemic homeostasis.

**Keywords**

Subcutaneous fascia, Metabolic reprogramming, Macrophages, Cd34+/Pdgfra+ telocytes, Deep learning

## Introduction

The classical paradigm of life as an integrated, homeostatic process posits that systemic alterations can profoundly influence cellular functions at peripheral and distal sites. The experimental evidence encompasses visceral obesity-induced subcutaneous adipocytic metabolic disorders and chronic inflammation-derived distal effects through the circulation system<sup>1</sup>. Despite widely reported inflammatory lesions-derived chemokine-mediated trafficking of myeloid cells across the bone marrow, spleen, and trans-endothelial recruitment<sup>2</sup>, the sophisticated biological process that recruited immune cells experienced on their way to the target organ is poorly revealed, conventional phenotypic investigations of disease pathogenesis have predominantly focused on localized changes within pathological tissues, resulting overlooking the broader implications of a holistic homeostatic framework.

Subcutaneous fascia, a ubiquitously distributed loose connective tissue, is richly populated by mesenchymal and immune cells, and extensively characterized in wound healing and angiogenesis<sup>3,4</sup>. Due to its intricate vascular, neural, and cellular architecture, scFascia is uniquely positioned to receive and integrate signals from visceral pathologies<sup>5,6</sup>. However, its role in orchestrating systemic homeostasis, particularly in the setting of inflammatory diseases, remains inadequately elucidated.

Salmonella enteritis, an acute gastroenteritis caused by invasive Salmonella infections, represents a complex pathological homeostasis involving the interplay between intestinal microbiota and cells within the digestive tract<sup>7</sup>. Upon invasion by aggressive pathogens, intestinal macrophages undergo Warburg metabolic reprogramming, characterized by decreased aerobic metabolism and disruption of the TCA cycle. This reprogramming is partially driven by the interference of normal cellular metabolism due to Salmonella's carbon source appropriation upon infiltrating macrophages<sup>8</sup>. Warburg reprogramming typically signifies an alteration in cellular energy supply<sup>9</sup>, commonly triggered by increased demands for DNA synthesis associated with cellular proliferation<sup>10</sup>, immune evasion<sup>11</sup>, and, in the context of tumor cells, the promotion of dedifferentiation<sup>12</sup>. These findings suggest that the emergence of Warburg reprogramming is indicative of enhanced proliferative capacity and complex immunological variations within cells<sup>7</sup>. This phenomenon is particularly salient in the context of the systemic inflammatory effects induced by Salmonella enteritis, where acute inflammation often prompts a more aggressive modulation of immune cell proliferation and supply to effectively counteract pathogenic threats<sup>13</sup>.

In this study, we established a Salmonella-induced enteritis model in Sprague-Dawley (SD) rats to investigate the systemic impact of visceral inflammation on scFascia. We delineated the transcriptional alterations of scFascia cell populations in response to visceral disease, utilizing scRNA-seq and neural network-based deep learning analyses. This integrative approach revealed the hitherto unrecognized homeostatic regulatory potential of scFascia and its cellular functional relevance in systemic inflammatory pathologies, thereby underscoring its significance as a critical mediator of whole-body homeostasis, and making it possible to apply scFascia characteristics to visceral disease diagnosis.

## Results

### **Salmonella-induced dysentery elicits alterations of cellular proportion and inflammatory phenotype of gene expression profiles in scFascia.**

In this study, we generated the expression matrix using Cell Ranger version 7.2.0. A total of 30,388 high-quality single-cell samples were obtained from the scFascia of the healthy group (HG: HG\_1 and HG\_2, n=13,224) and dysentery group (DG, DG\_1 and DG\_2, n=17,164). Interstitial and immune cells were annotated in both cohorts, and all cell types were distinctly distributed in UMAP coordinates, with variations reflecting different cellular states (Figure. 1A). No batch correction was required because the principal component analysis (PCA) reduction correlated to the cell type annotations (Supplementary Figure. 1A, B). The cellular populations within the fascia were annotated into 12 distinct types (Figure 1A, B, E). To validate the presence of macrophages and CPTCs, we performed immunofluorescence staining for Cd34/Pdgfra and F4/80 in the subcutaneous fascia, revealing a spatially parallel distribution pattern of these cell types within the scFascia tissue (Figure 1A1, D). Histopathological examination of the colon, the target site of modeling, demonstrated vascular congestion and infiltration following Salmonella gavage, but no significant damage to the mucosal epithelium was observed (Figure 1C).

To obtain an overarching preliminary assessment, we categorized all annotated cells into six major groups: myeloid cells (MCs), CPTCs, endothelial cells (ECs), fibroblasts (FCs), lymphocytes (LPs), and erythrocytes (ETCs) (Figure. 2). Differential gene expression (DGE) analysis was performed between dysentery and healthy groups for each cell type, followed by Gene Set Enrichment Analysis (GSEA). The results revealed that these cell types collectively exhibited similar inflammatory signatures and patterns of pathogen-associated molecular pattern (PAMP)-driven innate immune responses. By extracting and comparing the top three GSEA GO terms based on normalized enrichment scores (NES), we observed that these cells broadly shared inflammatory response characteristics, with some cell types displaying overlapping functional annotations (Figure. 3E). For instance, both mural cells (MuCs) and ECs showed activation in response to lipopolysaccharide (LPS), while MCs and MuCs exhibited responses to bacterial-derived molecules. This confirmed that the challenge had systemically elevated the concentration of PAMPs, such as LPS, within the circulatory system<sup>14</sup>.

Furthermore, the proportion of MuCs was significantly upregulated in the dysentery group (Figure. 1B), with upregulated genes including *Cc/2* and *//6* associated with inflammation and chemotaxis<sup>15</sup> (Supplementary Table. 1). Given the cellular composition of the perivascular microenvironment in scFascia (Figure. 2), we hypothesize the presence of a pathological macrophage-associated microenvironmental homeostasis, akin to findings in prior studies<sup>15</sup>. These observations suggest that scFascia may play a role in distal immune regulation during visceral infection and inflammation.

### **Deep learning reveals impaired aerobic respiration in scFascia MPs and identified potential crosstalk with CPTCs in dysentery.**

To delineate the most direct transcriptional alterations within scFascia cells under Salmonella-induced dysentery conditions, we partitioned the scFascia population into 6

major cellular subsets, including myeloid cells, lymphocytes, fibroblasts, CPTCs, mural cells, and erythrocytes. Expression matrices were generated for each cell type and annotated with labels corresponding to their respective treatment groups. These matrices were subsequently utilized as input for a deep learning framework based on a neural network model (Figure. 2). We identified the optimal model through iterative training and employed DeepSHAP<sup>16</sup> to extract interpretable features (Figure. 3A, B, C), including key signature genes, to elucidate the underlying transcriptional dynamics.

Comparative analysis of these genes with Gene Set Enrichment Analysis (GSEA) enrichment derived from directly computed differentially expressed genes (DEGs) revealed significant discrepancies in cellular functions between the two approaches (Figure. 3D). By extracting the top three GSEA terms associated with the highest activity levels for each cell type under dysentery conditions, we observed that myeloid cells within the scFascia exhibited upregulation of hypoxia-responsive genes (Figure. 3F). At the same time, CPTCs displayed functional enrichment related to the regulation of myeloid cell differentiation (Figure. 3F). We conducted transmission electron microscopy (TEM) imaging of scFascia, to investigate the potential for functional interactions between these cell types. The results revealed that macrophages and CPTCs are frequently localized in the perivascular region, forming a composite structure alongside pericytes and other fibroblasts (Figure. 3G). Notably, morphological evidence of functional interactions between macrophages and CPTCs was observed (Figure 3G). These findings suggest that specific regulatory signals between CPTCs and myeloid cells may underlie the alterations in cellular respiratory functions in myeloid cells under dysentery conditions.

### **MPs of scFascia in the DG exhibit augmented proliferative potential and Warburg metabolic reprogramming.**

To investigate how aerobic respiration-related cellular functions in myeloid cells influence metabolic pathways, we isolated myeloid cells from the overall scFascia single-cell dataset and re-annotated them based on canonical immune markers specific to MPs and treatment groups (Figure. 4B, D). Unsupervised clustering partitioned MPs into four distinct subpopulations (Figure. 4A, C), upon which we performed single-cell metabolic pathway analysis using the scMetabolic tool<sup>17</sup>. This analysis revealed that MPs, which constitute the majority of myeloid cells in the scFascia, exhibited significant downregulation of the tricarboxylic acid (TCA) cycle, and upregulation of gluconeogenesis pathways under dysentery conditions compared to the healthy control group (Figure. 5A). This MPs' metabolic alteration mirrors the Warburg phenotype observed during enteric bacterial infections<sup>7</sup>, typically indicative of adaptive homeostatic adjustments in response to enhanced cellular proliferation<sup>9,18</sup>.

Further analysis of the cell cycle distribution within MPs demonstrated a marked reduction in the proportion of cells in the G1 phase and a concurrent increase in the S phase under dysentery conditions compared to the healthy group (Figure. 5E). These findings suggest that salmonella dysentery significantly enhanced DNA replication and proliferative capacity among scFascia MPs.

### **Visceral inflammation induced cell state alterations of conventional M2 subsets in**

## **MPs.**

We conducted an in-depth analysis of macrophage subpopulations to elucidate further the core factors underlying the functional changes in scFascia macrophages induced by dysentery. We identified a subset of Gdf15+ macrophages in the dysentery group that co-expressed Cd163, a canonical marker of M2 macrophages. The UMAP distance between these Gdf15+ macrophages and Cd163+ cells from the HG was greater than their distance to other macrophage subsets, suggesting a distinct phenotypic divergence. Furthermore, the proportion of Gdf15+ macrophages was significantly elevated in the DG compared to the HG (Figure. 4C), indicating that these cells may represent a unique macrophage state specific to the disease condition.

Cytotrace analysis of cellular differentiation states revealed that Gdf15+ macrophages in the DG exhibited the highest degree of differentiation (Figure. 5B), implying that their functional specialization was more pronounced than that of their counterparts in the HG. We noticed that Fxyd5 and S100a11 were highly correlated to Cytotrace order as interpreted (Figure. 5D), both genes are the potential downstream responsive effect to Fgf/Wnt signal<sup>19-21</sup>. Fxyd5 has been proven to regulate cell proliferation and differentiation via the Akt/mTOR pathway, which is cross-regulatory with the Wnt/Fgf signal pathway<sup>20</sup>. Analysis of the top highly expressed genes in this subset demonstrated significant activation of pathways related to cellular responses to fibroblast growth factor stimuli and Wnt-mediated cell-cell signaling (Figure. 4E). Genes associated with hypoxia stress response, cellular proliferation, and inflammation were markedly upregulated (Figure. 4F, Supplementary Table. 2).

## **The intercellular communication network within scFascia under dysentery conditions exhibited an upregulation of macrophage proliferation and metabolic reprogramming mediated by CPTC-derived signaling.**

We performed CellCall<sup>22</sup> analysis to interrogate intercellular communication within the scFascia microenvironment to delineate further the potential crosstalk mechanisms underlying these observations. The results revealed that CPTCs exhibited robust signaling activity toward macrophages (Figure. 6A), with overall signaling intensity significantly higher in the dysentery group compared to the healthy group. Prominent ligand-receptor interactions included Wnt2/Wnt5a-Lrp6, Fgf10-Fgfr1, and Rspo3-Znrf3 (Figure. 6B, C, D). Additionally, fibroblasts in the dysentery group uniquely communicated with macrophages via the Rspo1-Znrf3 signaling axis (Figure. 6B, C, D). These interactions predominantly implicated the Wnt/Fgf signaling pathways, previously associated with enhancing cellular proliferation.

By dissecting the communication patterns of macrophage subpopulations, we identified Gdf15+ macrophages as the primary recipients of Wnt/Fgf pathway signals in the dysentery group (Figure. F). Intriguingly, these macrophages also exhibited gene expression profiles reminiscent of host response pathways activated during intestinal Salmonella infection (Supplementary Table. 3). We hypothesize that this distal metabolic reprogramming is not directly caused by Salmonella infection but rather mediated through secondary signaling mechanisms.

We employed PySCENIC<sup>23</sup> to infer transcription factor (TF) activity from the scFascia

single-cell expression matrix to explore the underlying regulatory drivers. Analysis of MP TF activity revealed significant upregulation of three TFs downstream of Wnt/Fgf signaling in the dysentery group: *Fosl1*, *Nfkb2*, and *Atf4* (Figure. 6E, Figure. 7A). To validate the functional relevance of these TFs, we extracted and compared the expression of their target genes between groups. Differential expression analysis followed by GSEA demonstrated that these target genes were significantly enriched for functions related to cellular proliferation and DNA replication in the DG, while functions associated with aerobic respiration were markedly downregulated (Figure. 7B, C). This result validated our hypothesis of CPTC signal-induced upregulation of MP proliferation in scFascia of DG.

### **The transcriptional profile of scFascia cells exhibits significant potential as a diagnostic tool for visceral diseases.**

To demonstrate that the whole-cell expression profile of scFascia undergoes significant and discernible changes under disease conditions and that these changes are sufficiently robust to be captured by neural networks, we partitioned the biological samples into two distinct pairs: Group 1 (G1), comprising DG\_1/HG\_1, and Group 2 (G2), comprising DG\_2/HG\_2. Each group consisted of samples derived from independent biological replicates. Labeled whole-cell expression matrices were generated for both groups, and cross-validation was performed to evaluate the predictive accuracy and generalization capability of the trained models on unseen data (Supplementary Figure 1C, D).

Remarkably, the models trained on each group exhibited exceptional generalization performance when applied to the opposing group's dataset. Specifically, the G1 model achieved an accuracy of 96.44% on the G2 test dataset, while the G2 model demonstrated an accuracy of 98.47% on the G1 test dataset (Figure 7D, E, F). These results underscore the robustness and reproducibility of scFascia expression profiles as a reliable biomarker for disease states, as well as the efficacy of neural networks in capturing and generalizing these patterns across independent biological replicates.

### **Discussion**

In this study, *Salmonella* dysentery induced transition of expression profile in the scFascia cell types, proving that visceral inflammation may influence the cell state located distally on a significant scale. Specifically, each cell type in the scFascia served a different role in the view from the deep-learning framework. These functional insights are attributable to the capability of deep learning to uncover nonlinear relationships between data features and labels<sup>24</sup>. The single-cell sequencing data used in this study encompass complex biological processes, they are typically characterized by significant nonlinear relationships and intricate effects that require advanced analytical approaches for identification<sup>25</sup>.

MPs and CPTCs as the predominant cytological components were revealed with an FVICP under dysbiosis conditions, in this study, FVICP can concluded with the following basic characteristics for the first time:

1. Systemic dissemination of visceral pathological signals: FVICP is underpinned by the systemic spread of pathological signals from visceral organs and the extensive

interaction between the circulatory system and the microenvironment in remote responding tissues.

2. Synchronization and mapping of immune states: The immune status of certain visceral organ cells is mirrored in distal tissues. For instance, we observed Warburg-like metabolic reprogramming in scFascia macrophages during intestinal dysbiosis<sup>8</sup>.

3. Pathological homeostasis in distal microenvironments: Remote local immune microenvironments establish a corresponding pathological equilibrium in response to visceral dysregulation.

Leveraging distal single-cell transcriptional profiles under dysbiosis conditions, this study reveals that scFascia can reflect visceral pathological changes during intestinal microbiota dysregulation. This finding aligns with the concept in traditional Chinese medicine wherein meridians reflect visceral states on the body's surface<sup>26</sup>. Using an MLP model, we successfully executed a simple yet highly accurate binary classification task. We propose that scFascia, as a pervasive connective tissue, mediates the correlation between superficial tissues and visceral organs, serving as a sensitive indicator of systemic homeostasis under various pathological conditions. By integrating systemic homeostasis data across diverse disease models and constructing larger classification frameworks, this approach holds significant potential for the development of rapid and precise systemic diagnostic technologies leveraging large-scale, commercially available sequencing platforms.

## **Methods and material**

### **Ethical approval**

The experimental subjects, female Sprague-Dawley rats aged eight weeks and weighing approximately 250 grams, were obtained from Beijing Vital River Laboratory Animal Technology Co., Ltd. Ethical clearance for all animal-related experimental protocols was secured from the Institutional Animal Care and Use Committee (IACUC) of Nanjing Agricultural University, under protocol number NJAU.No20220427087. These studies strictly adhered to the IACUC's guiding principles and aligned with the ARRIVE (Animal Research: Reporting In Vivo Experiments) guidelines. The rodents were housed in a fully ventilated cage system ensuring unrestricted access to food and water. Environmental conditions were stringently maintained with a stable ambient temperature of approximately 25°C and a natural light-dark cycle to simulate the animals' native habitat.

### **Bacterial strains and growth conditions**

The *Salmonella* Typhimurium strain CVCC542 (hereafter referred to as *S. Typhimurium* CVCC542) was obtained from the Joint International Research Laboratory of Animal Health and Food Safety. The cultivation process was conducted in Luria-Bertani (LB) broth (BeyoPure, Cat. Number: ST156), supplemented with 50 µg/mL kanamycin, at 37°C. Initial culturing involved overnight incubating in a 2-mL static culture at 37°C to enrich the motile bacteria. Subsequently, the upper 1 mL of this culture was transferred into 49 mL of preheated LB broth and subjected to shaking incubation for 5 hours at the same temperature. The optical density of the *S. Typhimurium* culture was assessed at 600 nm using an Eppendorf BioPhotometer plus to ascertain the bacterial concentration. An appropriate bacterial dose was then prepared in sterile 0.01 M phosphate-buffered saline (PBS) with a pH of approximately 7.4.

### **Animal assays**

Six female Sprague-Dawley (SD) rats, aged eight weeks with an average body weight of 250g, were subjected to a 3-day oral gavage regimen to induce *Salmonella* Typhimurium infection. The bacterial suspension was adjusted to a concentration of  $5 \times 10^8$  colony-forming units per milliliter (CFU/mL) using 0.01 M PBS. To neutralize gastric acidity prior to infection, the dysentery group received an oral dose of 5% sodium bicarbonate ( $\text{NaHCO}_3$ ). Ten minutes later, 400 µL of the bacterial suspension was administered via gavage. This procedure was repeated every 24 hours for three consecutive days at 2:00 PM. The HG consisting of an additional six SD rats, was maintained on a standard diet without intervention.

### **Sampling**

This section delineates the methodological framework for preparing tissue samples of DG and HG, facilitating morphological analysis and single-cell sequencing investigations.

Procedures:

Sacrifice and Compliance:

All subjects were euthanized adhering to the Institutional Animal Care and Use Committee (IACUC) protocols and under ARRIVE guidelines to uphold ethical standards.

Morphological Studies:

Specimens, comprising intact skin and scFascia along the abdominal midline with a



width of 2cm from the pubic symphysis to the xiphoid, were harvested for paraffin sections and transmission electron microscopy analysis.

**Fixation:** Samples underwent fixation in a solution containing 4% paraformaldehyde and 0.25% glutaraldehyde in PBS, ensuring the preservation of cellular architecture for subsequent detailed morphological sample preparation and assessment.

**Preparation for Single-cell Sequencing:**

The scFascia was sampled along the abdominal midline with a width of 2cm from the pubic symphysis to the xiphoid, meticulously dissected to isolate it from surrounding dermal and adipose tissues.

**Storage:** To preserve cellular viability before tissue dissociation, specimens were maintained in a 0°C ice bath using a specialized tissue storage solution (Miltenyi Biotec, Catalogue No. 130-100-008).

### **Immunofluorescence (IF), Hematoxylin, and Eosin (HE) staining.**

The hydrated paraffin-embedded tissue sections underwent antigen fixation through incubation in 0.01 M sodium citrate at 98°C for 5 minutes. Post-incubation, sections were treated with primary antibodies, followed by fluorescently labeled secondary antibodies and DAPI staining (Beyotime, Cat. Number: C1005). Fluorescent images were acquired using a confocal microscope (Carl Zeiss, LSM900). Subsequently, sections were dehydrated for hematoxylin and eosin (HE) staining and preserved with neutral resin for extended storage.

**Antibodies Employed in This Investigation:**

Anti-CD34 (Abclonal, Cat. Number: A13929)

Anti-PDGFR $\alpha$  (Santa Cruz, Cat. Number: sc-398206)

Anti-F4/80 (Abcam, Cat. Number: Ab300421)

Alexa Fluor 488 Anti-Rabbit Fc Fragment (Proteintech, Cat. Number: SA00013-2)

Alexa Fluor 594 Anti-Mouse Fc Fragment (Proteintech, Cat. Number: SA00013-3)

### **Transmission Electron Microscopy (TEM)**

Fascia samples were initially fixed in a 2.5% glutaraldehyde solution for 48 hours at 4°C, followed by post-fixation in 1% osmium tetroxide for 2 hours under the same temperature conditions. The specimens underwent dehydration through a graded alcohol series, comprising concentrations of 75%, 85%, 95%, and 100%, each for 10 minutes. Subsequently, the tissues were embedded in epoxy resin. Ultrathin sections, approximately 50 nm thick, were mounted on copper grids and subjected to staining with uranyl acetate and lead citrate. The prepared sections were then analyzed using a Hitachi HT7800 transmission electron microscope operating at an acceleration voltage of 80 kV.

### **Tissue dissociation and cell purification for scRNA-seq**

Initially, the tissue was transferred from the Miltenyi storage solution into a sterile culture dish containing 10 mL of 1x Dulbecco's Phosphate-Buffered Saline (DPBS; Thermo Fisher, Catalogue Number: 14190144) on ice. This step was implemented to eliminate residual blood and adipose tissue, after which the tissue was finely minced on ice.

A specialized dissociation solution was prepared, comprising collagenase type 4 (Sigma-Aldrich, Catalogue Number: C5138), elastase (Sigma-Aldrich, Catalogue Number: E1250), and 10  $\mu$ g/mL DNase I (Thermo Fisher, Catalogue Number: EN0523), all dissolved in PBS supplemented with 5% Fetal Bovine Serum (FBS; Thermo Fisher, Catalogue Number: SV30087.02). The tissue was subjected to enzymatic digestion in this solution at

37°C with gentle agitation at 50 rpm for approximately 40 minutes. Dissociated cells were collected at 20-minute intervals to optimize cell yield and viability.

The resultant cell suspensions underwent sequential filtration through nylon cell strainers decreasing from pore sizes of 100 µm to 40 µm to remove debris. The remaining red blood cells were lysed using 1X Red Blood Cell Lysis Solution (Thermo Fisher, Catalogue Number: 00-4333-57). The dissociated cells were washed with 1x DPBS containing 2% FBS. Cell viability was assessed using 0.4% Trypan blue staining and confirmed with a Countess® II Automated Cell Counter (Thermo Fisher). Subsequently, cell suspensions were processed with the Dead Cell Removal Kit (Miltenyi Biotec, Catalogue Number: 130-090-101), ensuring that only samples with greater than 95% viability were advanced for further analysis.

To construct 10X libraries and 3' sequencing, suspension cells were prepared using a water-in-oil solution. This solution was crafted by the Chromium™ Single Cell Controller (10X Genomics), enabling high-fidelity capture and sequencing of individual cells.

#### 10X library construction

In this study, beads, each imbued with a unique molecular identifier (UMI) and cell barcodes, were loaded to near saturation, ensuring each cell was paired with a bead within a Gel Beads-in-emulsion (GEM). Upon exposure to a cell lysis buffer, polyadenylated RNA molecules hybridized to these beads, and subsequently collected into a singular tube for reverse transcription. During cDNA synthesis, each cDNA molecule was uniquely tagged at the 5' end, corresponding to the 3' end of an mRNA transcript, with a UMI and a cell-specific label. The beads underwent sequential processes of second-strand cDNA synthesis, adaptor ligation, and universal amplification. Sequencing libraries were prepared from randomly fragmented whole-transcriptome amplification products to enrich the 3' ends of transcripts associated with cell barcodes and UMIs, adhering to the standard protocol of the Chromium Single Cell 3' v3.1 system. The libraries were precisely quantified using both a High Sensitivity DNA Chip (Agilent) via a Bioanalyzer 2100 and the Qubit High Sensitivity DNA Assay (Thermo Fisher Scientific), culminating in sequencing on an Illumina NovaSeq 6000 platform using 2x150 bp read chemistry.

#### **scRNA-seq pipeline**

The expression matrix was generated by Cellranger 7.2.0, and the primary processing was executed using Seurat v4.4 within the R environment version 4.3.0. Following rigorous quality control and adherence to the standard Seurat pipeline, all single-cell RNA sequencing (scRNA-seq) data were stratified according to cell type annotations with DH and HG. The subsequent extraction of Seurat objects and processed matrices facilitated downstream analyses such as deep learning, PySCENIC inference, and cell communication investigations.

#### **Deep learning and model interpretation**

We annotated single-cell sequencing data from subcutaneous connective tissue, comparing DG and HG. The expression matrices for each cell population were normalized, scaled, and labeled for binary classification tasks. During the training phase, a primary class of MLP class was defined at first, and an extensive parameter search for batch size, hidden layers, activation functions, and optimizers, was conducted to identify the optimal model parameters based on validation dataset performance. These parameters were then

used to generate models for subsequent interpretation and visualization. Model interpretation employed the DeepSHAP<sup>27</sup> method, ranking feature genes by their contribution to model accuracy. Genes with SHAP values were filtered and used to refine differentially expressed gene (DEG) lists, which were subsequently subjected to Gene Set Enrichment Analysis (GSEA) to identify biologically relevant functions uncovered by deep learning.

In cross-validation experiments using whole fascia single-cell data, biological replicates were isolated, and the expression matrices for the entire scFascia were processed identically to generate models. To assess generalization performance, models trained on one biological replicate were tested on datasets from other replicates, serving as unseen data. The results were visualized using confusion matrices to evaluate classification accuracy.

### **PySCENIC regulon network inferring**

scFascia and colon count matrix was generated from Seurat object after quality control as the input dataset, all procedures are guided as the GitHub project of PySCENIC (<https://github.com/aertslab/pySCENIC>).

### **Cell communication analysis**

We applied quality-controlled Seurat objects of scFascia and colon from each group to generate Cellcall objects following the guide of this GitHub project (<https://github.com/ShellyCoder/cellcall>).

### **Acknowledgments**

We extend our sincere gratitude to Professor Xu-Dong Zhu of Nanjing Agricultural University for his generous assistance and invaluable contributions throughout the course of this study. We also acknowledge the financial support provided by the National Natural Science Foundation of China (NSFC) under grant number 31872433, which made this research possible.

## References

- 1 Alexaki, V. I. Adipose tissue-derived mediators of systemic inflammation and metabolic control. *Current Opinion in Endocrine and Metabolic Research* **37** (2024). <https://doi.org/10.1016/j.coemr.2024.100560>
- 2 Shi, C. & Pamer, E. G. Monocyte recruitment during infection and inflammation. *Nature reviews. Immunology* **11**, 762-774 (2011). <https://doi.org/10.1038/nri3070>
- 3 Correa-Gallegos, D. *et al.* Patch repair of deep wounds by mobilized fascia. *Nature* **576**, 287-292 (2019). <https://doi.org/10.1038/s41586-019-1794-y>
- 4 Shi, Z., Yao, C., Shui, Y., Li, S. & Yan, H. Research progress on the mechanism of angiogenesis in wound repair and regeneration. *Front Physiol* **14**, 1284981 (2023). <https://doi.org/10.3389/fphys.2023.1284981>
- 5 Varghese, J. G. & Priya, G. Role of fascia in human function. *Research Journal of Pharmacy and Technology* **10**, 2759-2764 (2017).
- 6 Adstrum, S., Hedley, G., Schleip, R., Stecco, C. & Yucesoy, C. A. Defining the fascial system. *J Bodyw Mov Ther* **21**, 173-177 (2017). <https://doi.org/10.1016/j.jbmt.2016.11.003>
- 7 Tang, B., Cui, W., Li, X. & Yang, H. Salmonella—Host—microbiota interactions: Immunity and metabolism. *iMetaOmics* **1** (2024). <https://doi.org/10.1002/imo2.16>
- 8 Jiang, L. *et al.* Salmonella Typhimurium reprograms macrophage metabolism via T3SS effector SopE2 to promote intracellular replication and virulence. *Nature communications* **12**, 879 (2021). <https://doi.org/10.1038/s41467-021-21186-4>
- 9 Nath, S. & Balling, R. The Warburg Effect Reinterpreted 100 yr on: A First-Principles Stoichiometric Analysis and Interpretation from the Perspective of ATP Metabolism in Cancer Cells. *Function (Oxf)* **5**, zqae008 (2024). <https://doi.org/10.1093/function/zqae008>
- 10 Sun, P., Ma, L. & Lu, Z. Lactylation: Linking the Warburg effect to DNA damage repair. *Cell Metab* **36**, 1637-1639 (2024). <https://doi.org/10.1016/j.cmet.2024.06.015>
- 11 Chen, J. *et al.* Warburg Effect Is a Cancer Immune Evasion Mechanism Against Macrophage Immunosurveillance. *Frontiers in immunology* **11**, 621757 (2020). <https://doi.org/10.3389/fimmu.2020.621757>
- 12 Jiang, H., Jedoui, M. & Ye, J. The Warburg effect drives dedifferentiation through epigenetic reprogramming. *Cancer Biol Med* **20**, 891-897 (2024). <https://doi.org/10.20892/j.issn.2095-3941.2023.0467>
- 13 Xiong, D., Song, L., Chen, Y., Jiao, X. & Pan, Z. Salmonella Enteritidis activates inflammatory storm via SPI-1 and SPI-2 to promote intracellular proliferation and bacterial virulence. *Front Cell Infect Microbiol* **13**, 1158888 (2023). <https://doi.org/10.3389/fcimb.2023.1158888>
- 14 Violi, F. *et al.* Gut-derived low-grade endotoxaemia, atherothrombosis and cardiovascular disease. *Nature Reviews Cardiology* **20**, 24-37 (2022). <https://doi.org/10.1038/s41569-022-00737-2>
- 15 Pekayvaz, K. *et al.* Mural cell-derived chemokines provide a protective niche to safeguard vascular macrophages and limit chronic inflammation. *Immunity* **56**, 2325-2341 e2315 (2023). <https://doi.org/10.1016/j.immuni.2023.08.002>
- 16 Lundberg, S. M. & Lee, S.-I. in *Proceedings of the 31st International Conference on*

*Neural Information Processing Systems* 4768–4777 (Curran Associates Inc., Long Beach, California, USA, 2017).

- 17 Wu, Y. *et al.* Spatiotemporal Immune Landscape of Colorectal Cancer Liver Metastasis at Single-Cell Level. *Cancer Discov* **12**, 134–153 (2022). <https://doi.org/10.1158/2159-8290.CD-21-0316>
- 18 Kelly, B. & O'Neill, L. A. Metabolic reprogramming in macrophages and dendritic cells in innate immunity. *Cell research* **25**, 771–784 (2015). <https://doi.org/10.1038/cr.2015.68>
- 19 Meng, M., Sang, L. & Wang, X. S100 Calcium Binding Protein A11 (S100A11) Promotes The Proliferation, Migration And Invasion Of Cervical Cancer Cells, And Activates Wnt/beta-Catenin Signaling. *Onco Targets Ther* **12**, 8675–8685 (2019). <https://doi.org/10.2147/OTT.S225248>
- 20 Tan, X. P. *et al.* FXD5 promotes sorafenib resistance through the Akt/mTOR signaling pathway in hepatocellular carcinoma. *European journal of pharmacology* **931**, 175186 (2022). <https://doi.org/10.1016/j.ejphar.2022.175186>
- 21 Zhang, Y. *et al.* S100A gene family: immune-related prognostic biomarkers and therapeutic targets for low-grade glioma. *Aging (Albany NY)* **13**, 15459–15478 (2021). <https://doi.org/10.18632/aging.203103>
- 22 Zhang, Y. *et al.* CellCall: integrating paired ligand-receptor and transcription factor activities for cell-cell communication. *Nucleic acids research* **49**, 8520–8534 (2021). <https://doi.org/10.1093/nar/gkab638>
- 23 Kumar, N., Mishra, B., Athar, M. & Mukhtar, S. Inference of gene regulatory network from single-cell transcriptomic data using pySCENIC. *Modeling Transcriptional Regulation: Methods and Protocols*, 171–182 (2021).
- 24 Olivieri, A. C. in *Introduction to Multivariate Calibration* Ch. Chapter 14, 271–288 (2024).
- 25 Heil, B. J., Crawford, J. & Greene, C. S. The effect of non-linear signal in classification problems using gene expression. *PLoS computational biology* **19**, e1010984 (2023). <https://doi.org/10.1371/journal.pcbi.1010984>
- 26 Jiang, Y. *et al.* Specificity for the correlation between the body surface and viscera in the pathological state of COPD: A prospective, controlled, and assessor-blinded trial. *Frontiers in Physiology* **14** (2023). <https://doi.org/10.3389/fphys.2023.1051190>
- 27 Pezoa, R., Salinas, L. & Torres, C. Explainability of High Energy Physics events classification using SHAP. *Journal of Physics: Conference Series* **2438**, 012082 (2023). <https://doi.org/10.1088/1742-6596/2438/1/012082>

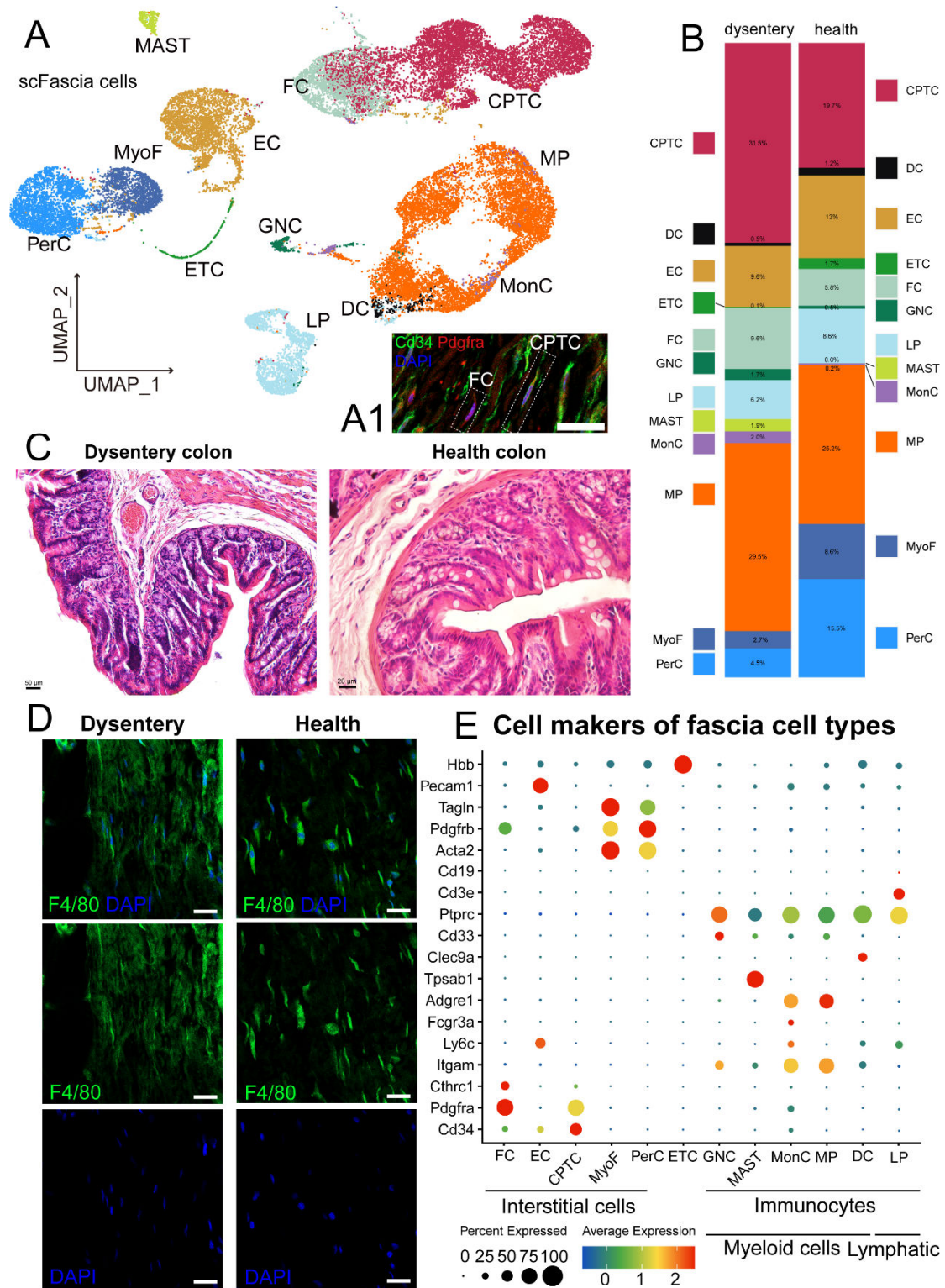


**Figure.1 UMAP Visualization of scRNA-Seq Data from Subcutaneous Fascial Tissues in Dysentery and Healthy Conditions**

A. UMAP projection of scRNA-Seq data from subcutaneous fascial tissues of rats with *Salmonella*-induced dysentery and healthy controls, illustrating the separation of cellular clusters based on disease status.

A1. Validation for cell markers of CPTCs and FCs with IF assays in scFascia.

- B. Percentage of cells expressing each gene, indicating the prevalence of specific markers in different cell populations between dysentery and healthy conditions.
- C. HE stained colonic pathological alteration in salmonella dysentery.
- D. MPs in the scFascia of dysentery and health groups,
- E. Average expression levels of the highlighted genes in the identified cell populations, highlighting differential expression associated with cell types.



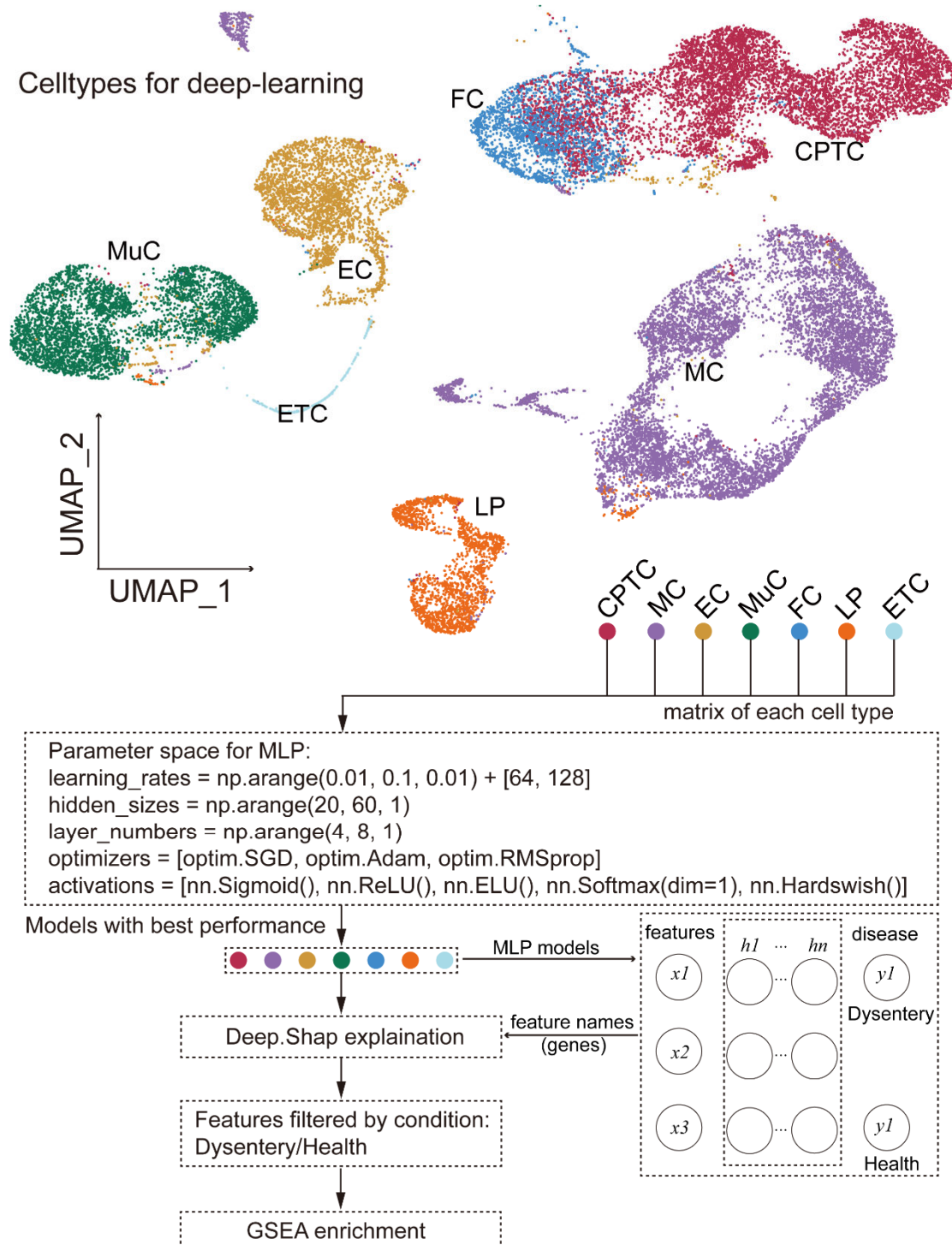


**Figure 2. Schematic overview of the deep learning pipeline implemented in this study.**

All cell types were systematically clustered and annotated with enhanced precision to facilitate robust deep-learning analysis. The primary distinctions from detailed annotations were observed in myeloid cells (MC, encompassing macrophages, mast cells, monocytes, granulocytes, and dendritic cells) and mural cells (MuC, including myofibroblasts and pericytes). Expression matrices derived from each cell type were subsequently utilized in a classification task to discriminate cells originating from dysentery and healthy cohorts. These classifications were further



interpreted through gene-level analysis and Shapley (SHAP) values. Gene Set Enrichment Analysis (GSEA) was conducted based on differentially expressed genes (DEGs) identified from the interpretation phase. The optimization of model performance was achieved through a hyper-parameter grid search strategy, ensuring the identification of optimal configurations for the deep learning framework.

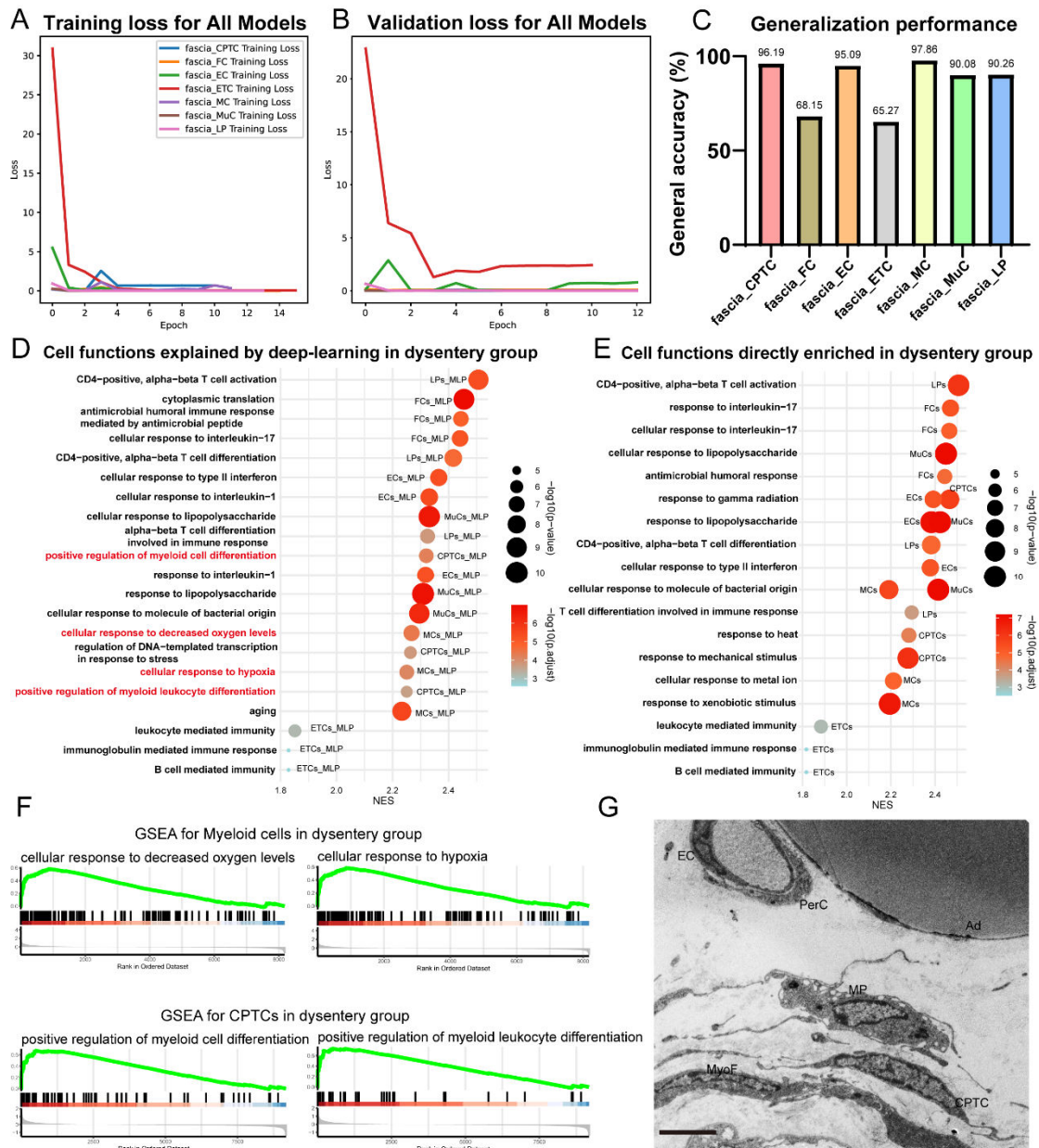


**Figure 3. Cell functions extracted through deep learning based on a neural network model.**

A. Training epochs and loss values for each cell population during deep learning.

B. Validation loss values for each cell population across training epochs.

C. Generalization performance of the optimal models for each cell population when applied to the full scFascia dataset.

D. Top Gene Set Enrichment Analysis (GSEA) terms derived from filtered gene symbols extracted using the DeepSHAP algorithm, following the calculation of intergroup expression differences.

E. Top GSEA terms obtained from directly computed differentially expressed genes (DEGs) for each cell population.

F. GSEA enrichment distribution for myeloid cells (MCs) and CPTCs.

G. Cellular composition of the perivascular microenvironment in scFascia under dysentery conditions.

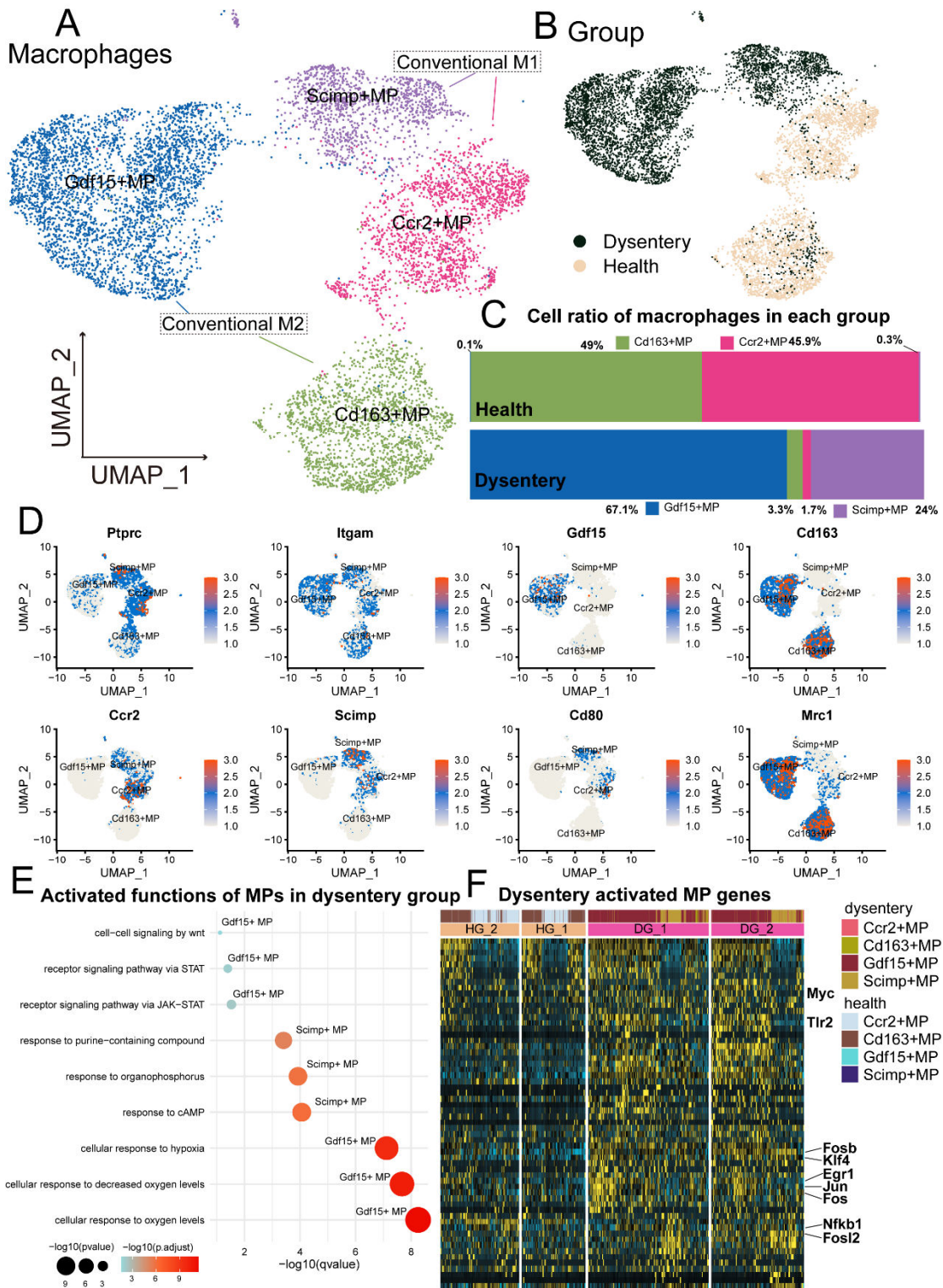


**Figure 4. Macrophage subpopulations and their functional characteristics.**

A. Annotation of MP populations based on characteristic markers.

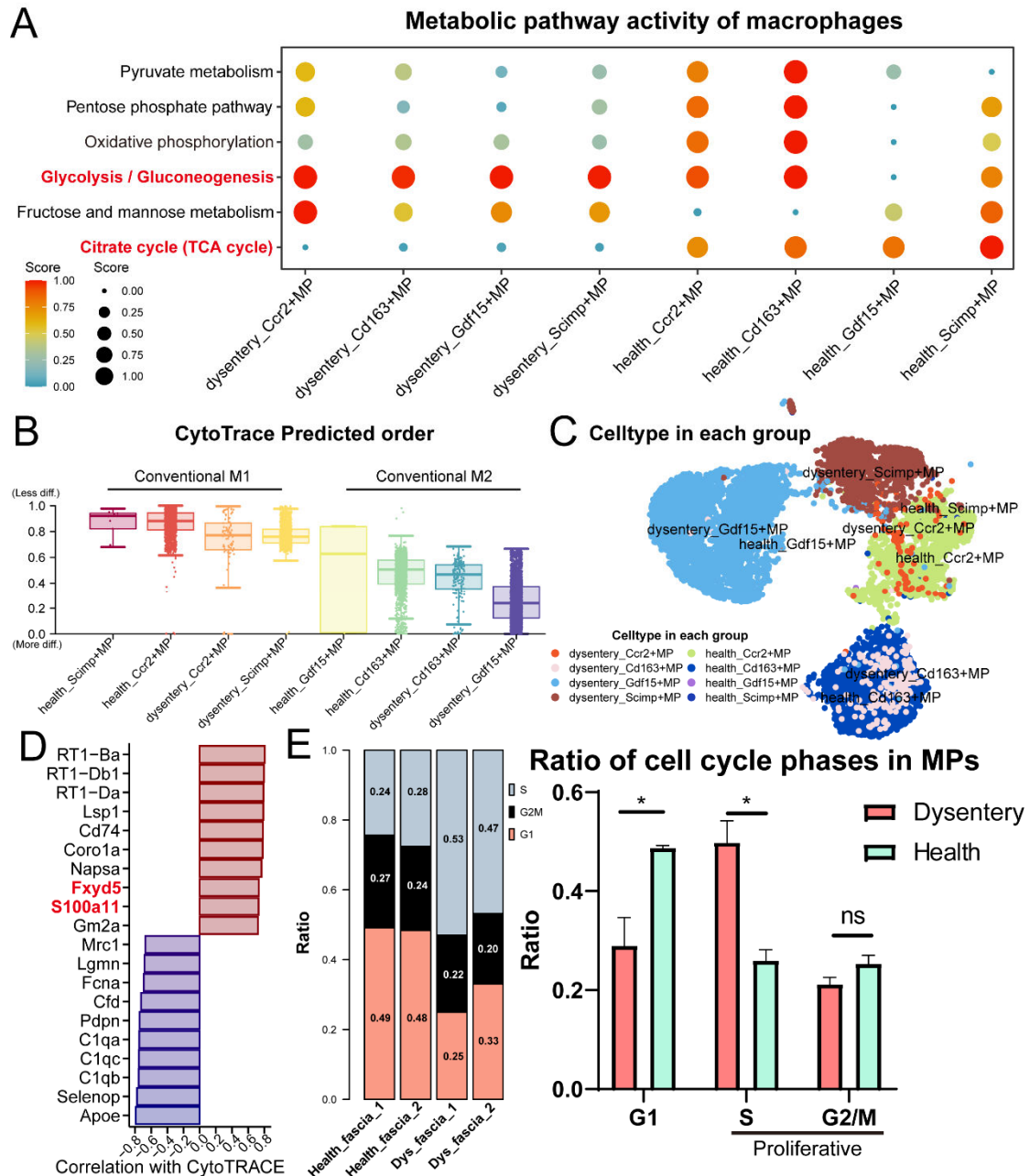
B. MP populations annotated according to group-specific differences.

C. Proportion of marker-specific macrophage subsets within each group.

D. Expression of classical immune markers and group-specific genes in MPs.

E. DG-specific upregulated cellular functions in MPs exhibiting classical M2 characteristics.

F. Heatmap showing the expression of genes associated with the functions highlighted in panel E across the entire macrophage population.





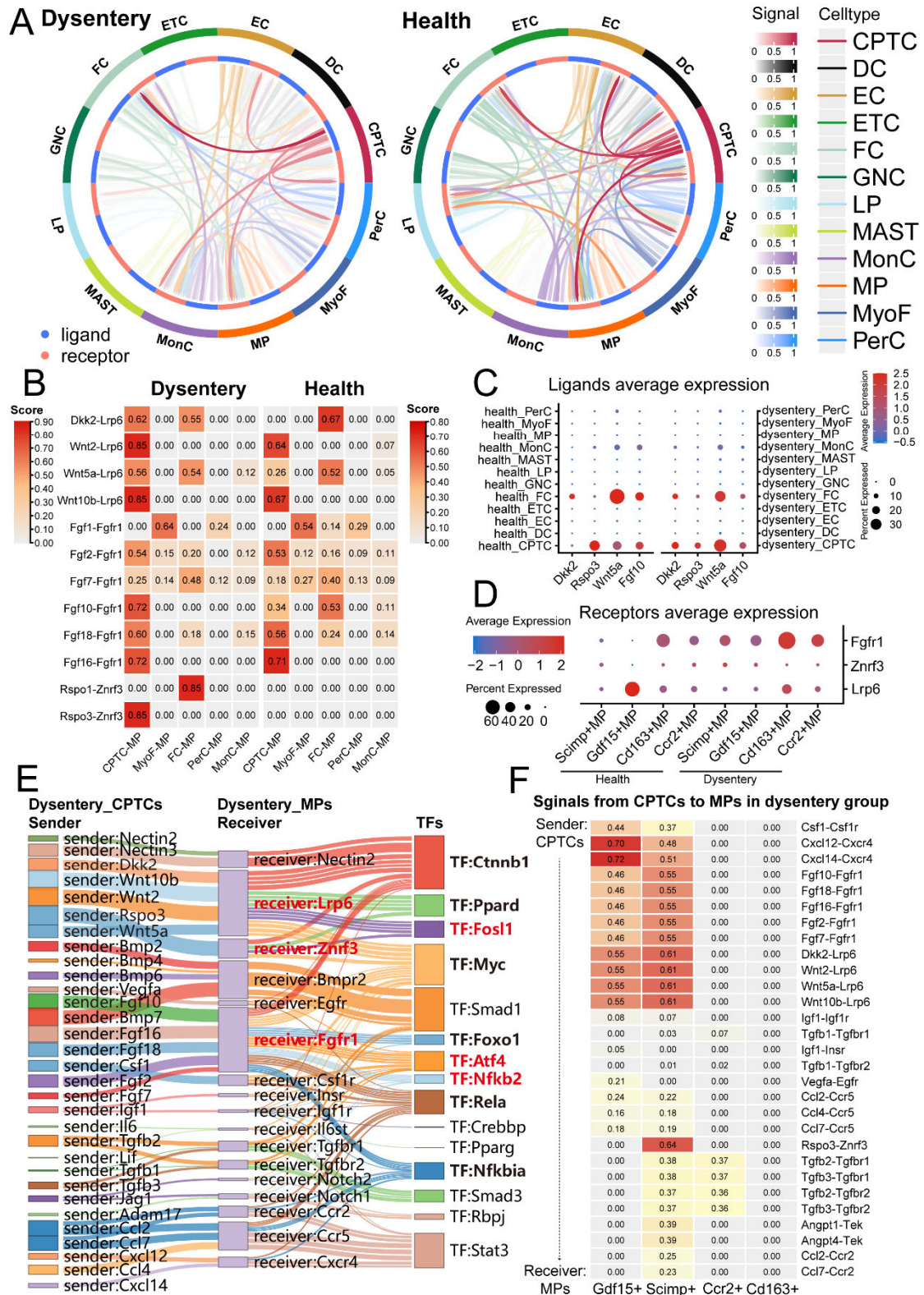


**Figure 6. Cell-cell communication analysis between MPs and CPTCs.**

A. Global visualization of cell-cell communication in scFascia from both groups, with arrow color intensity representing signal strength.

B. Heatmap dissecting Wnt/Fgf signaling, highlighting differences in intercellular communication between groups; darker colors indicate stronger downstream effects.

C. Expression levels of ligand genes associated with the interactions shown in panel B.

- D. Expression levels of receptor genes associated with the interactions shown in panel B.
- E. Sankey diagram illustrating cell-cell communication between CPTCs and MPs, depicting ligands, receptors, and downstream transcription factors from left to right.
- F. Heatmap of CPTCs-MPs communication after stratifying macrophage subpopulations, with color intensity representing the strength of downstream effects induced by each signal.

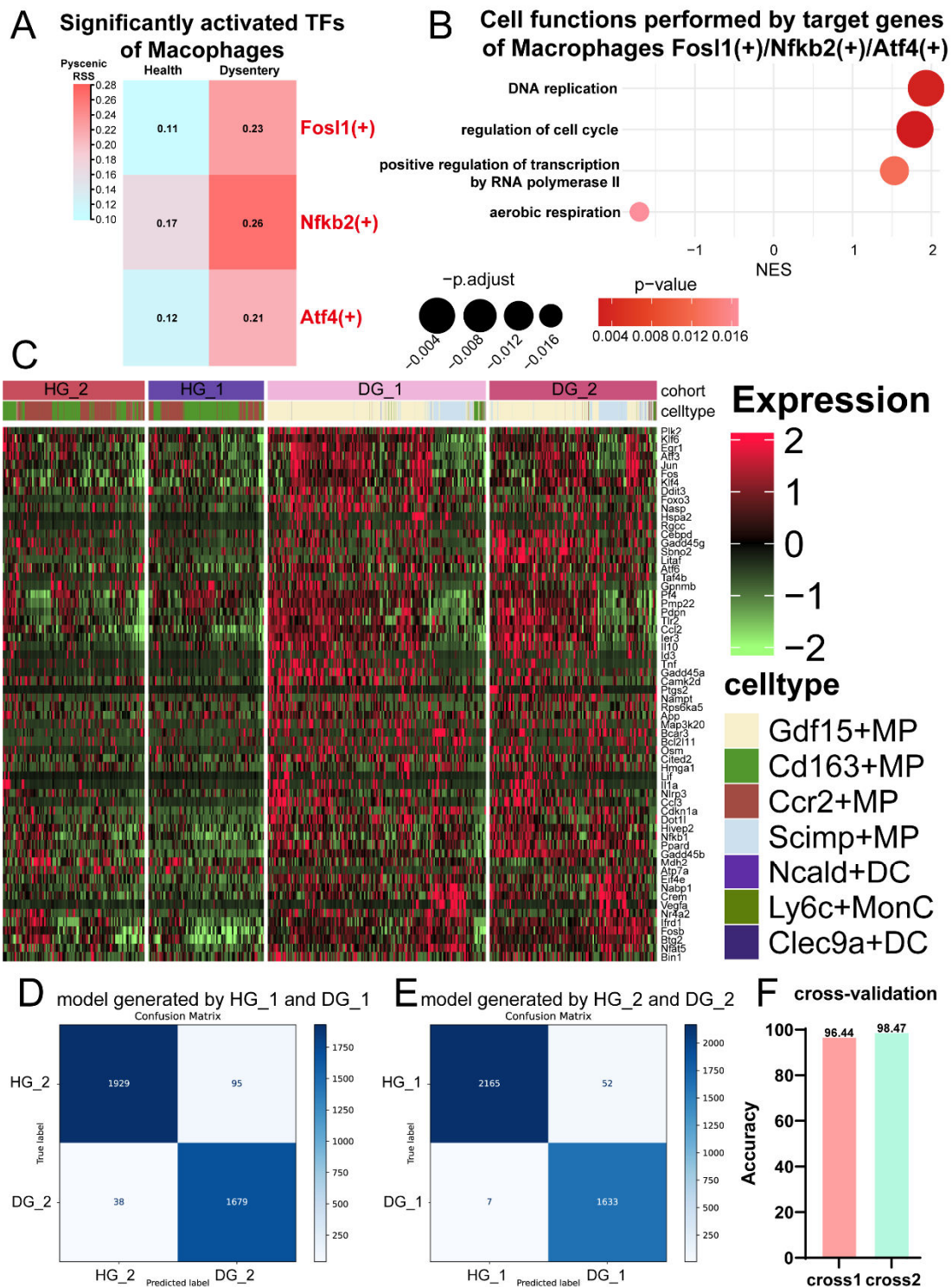


**Figure 7. PySCENIC analysis of downstream transcription factors (TFs) in macrophages and cross-validation of classification models trained on whole fascia data.**

A. Heatmap of PySCENIC analysis results for TFs downstream of Wnt/Fgf signaling in CPTCs-MPs interactions, with color indicating TF activity. RSS: Regulon Specific Score.

B. GSEA functional enrichment of target genes downstream of the TFs highlighted in panel A, specific to the dysentery group.



- C. Heatmap showing the expression of genes associated with the functions in panel B across all MPs.
- D. Confusion matrix for cross-validation of the model trained on the full scFascia expression matrix from the first biological replicate of DG and HG.
- E. Confusion matrix for cross-validation of the model trained on the full scFascia expression matrix from the second biological replicate of DG and HG.
- F. Generalization performance (accuracy) of both models during cross-validation.